ADVANCED MATERIALS INTERFACES
Open Access
www.advmatinterfaces.de

Multiplexed Bio-detection on an Interferometric Optical Waveguide Assembly

*Oleksii Bratash, Rémi Courson, Laurent Malaquin, Thierry Leichle, Arnaud Buhot, Loïc Leroy, and Elodie Engel**

Multiplexed remote bio-detection is demonstrated through an optical waveguide assembly coated with interferometric layers. Image conduits (IC)s, composed of 3012 individual cores, are coated with interferometric layers of tantalum pentoxide (Ta_2O_5) and silica (SiO_2) to transform each core into a sensitive sensor. The spectral response of the IC as a function of refractive index (RI) changes is obtained and compared with the simulated one. The experimental sensitivities and resolutions of individual cores of the waveguide are assessed in remote detection mode by imaging through the optical assembly. For 75% of the cores, a sensitivity better than 510%. RIU^{-1} (RI Unit) is obtained, corresponding to a resolution better than 7×10^{-4} RIU. Furthermore, the coated face of IC is functionalized with two localized arrays of hundred-micrometer droplets containing two different oligonucleotide (ODN) probes using a polymeric 3D-printed microcantilever. Hybridization of complementary ODN strands is detected for one of the probes, the second being a negative control. Interaction kinetics are monitored in functionalized areas by grouping several cores or on individual cores. Thus, multiplexed bio-detection on the surface of an interferometric waveguide is demonstrated for the first time paving the way for applications in multiplex in situ biosensing, and, ultimately, in vivo endoscopic diagnosis.

1. Introduction

When medical imaging combined with biochemical analysis of biological fluids (typically blood analysis) proves insufficient to establish a diagnosis, it is necessary to perform biopsies. Far from being innocuous, biopsies have many drawbacks, including pain, risk of bleeding or infection, and delays in treatment due to sample preparation steps. To limit these drawbacks, researchers and physicians are developing less invasive techniques, including the use of fine, hollow needles,[1] sometimes combined with suction.[2] These needles can be guided by computers or robots,[3] with real-time imaging (Magnetic Resonance Imaging, ultrasound). Tissues are then analyzed in the laboratory. An even less invasive method has been gaining ground over the last ten years: liquid biopsy. Initially dedicated to the early identification of cancerous pathologies from circulating tumor cells,[4] it is now being extended to other targets such as extracellular vesicles or nucleic acids present in patients' body fluids (blood, cerebrospinal fluid, urine).[5,6] Here too, analysis and diagnosis are delayed. Unlike needle biopsies, liquid biopsies are not localized. In this context, the use of optical fiber (OF) biosensors capable of performing multiplexed molecular in situ analysis, in real-time and without target labeling would ultimately enable faster (real-time), minimally invasive, and localized (in situ) analyses that could be coupled with imaging (via OF bundles). Implementing this "optical" biopsy offers enormous development potential for healthcare technologies, especially when diseased sites are difficult to access. This is the case for brain diseases whose evolution depends on the environment of the lesions.[7] Knowledge about this environment, which is difficult to reach by conventional biopsy, could prove to be useful in the treatment of associated pathologies. Although OFs are theoretically well suited to in vivo biosensing, they are not yet used in practice for such purposes. The main reason is that there is still a long way to go between laboratory experiments and the requirement of real medical applications. There are numerous fiber-based biosensors described in the literature, operating in transmission or reflection modes, which are based on different label-free transduction principles, such as surface plasmon resonance (SPR),[8,9] lossy mode resonances[10,11]

O. Bratash, A. Buhot, L. Leroy, E. Engel
Univ. Grenoble Alpes
CNRS, CEA, IRIG
SyMMES
Grenoble 38000, France
E-mail: elodie.engel@univ-grenoble-alpes.fr
R. Courson, L. Malaquin, T. Leichle
LAAS-CNRS, Université de Toulouse
CNRS
Toulouse 31400, France
R. Courson
Ifremer
RDT Research and Technological Development
Plouzané F-29280, France
T. Leichle
Georgia Tech—CNRS International Research Laboratory
Atlanta, GA 30332, USA

The ORCID identification number(s) for the author(s) of this article can be found under https://doi.org/10.1002/admi.202400941

DOI: 10.1002/admi.202400941

or interferometric.[12,13] For a general review of the use of OF in label-free biosensing, the reader may refer to the following papers.[14,15] Among this variety of fiber-based biosensors, those having a sensitive zone at the fiber tip are the most suitable for in vivo molecular diagnostics. Indeed, one significant advantage of the tip-based sensing approach is that the biosensor works in reflection mode, where the molecular recognition element is immobilized at the tip of the fiber, allowing the biosensor on the OF to be easily placed at the exact site of disease. In this case, detection is more localized and limited by the fiber tip or core size. Focusing solely on this particular configuration and interferometry-based biosensors, we can mention several devices that have demonstrated proof of concept for biosensing. For example, Wang et al. spliced one of the ends of a thin-core fiber with a single-mode fiber and then melted the opposite end of the thin-core fiber to form a rounded tip.[16] The functionalized tip of the fiber biosensor was validated for glucose detection in the 10 µM–10 mM range. Configuration closer to conventional Michelson interferometer was developed on the basis of dual-core fiber.[17] One core was functionalized with antibodies, whereas the second played the role of reference. The antigen binding to the antibodies, considered as an increase in the optical path, led to phase modulation, allowing the detection of 160 µg mL^{-1} of rabbit IgG. Wang et al. proposed a Fabry-Perot interferometer (FPI) biosensor with a multilayer functional structure composed of epoxy resin and graphene oxide layers. Beta-cyclodextrin was chemically bonded to the latter layer to detect cholesterol with a limit of detection (LOD) estimated at 3.48 µM.[18] In a recent example, Tang et al. proposed an interesting approach using two-photon printing technology.[19] They deposited a photoresist on the tip of a single-mode OF, which underwent photopolymerization, forming a bridge-like open structure. The fabricated structure formed an open cavity accessible to the tested medium and was implemented for the detection of glucose having LOD equal to 0.45 mg mL^{-1}. Commercially available interferometric fiber biosensors, often referred to as biolayer interferometry biosensors, use an FPI approach, such as the Octet biosensors from Sartorius (formerly ForteBio).[20] These biosensors have been used to detect various substances in vitro, including Tau441 protein, Testosterone, Glucose, and Gonyautoxin 1/4, with very good LOD values (6.7 nM,[21] 2.13 ng mL^{-1},[22] 0.45 mg mL^{-1},[23] and 50 pg mL^{-1},[24] respectively). Very recently, Burnat et al. improved on this multi-layer system by proposing an FPI cavity formed by two thin films, enabling discrimination of RI changes in volume or on the sensor surface. By adapting the materials and thicknesses of the two layers, they optimized their sensor to detect an inflammation marker, the myeloperoxidase, with an LOD of 10^{-11} g mL^{-1}.[13] All the previously described biosensors demonstrated their ability to detect a single analyte per fiber. However, if these sensors are ever to be used for in vivo diagnostic purposes, compact, localized, and multiplexed detection (of several biomarkers and including controls) is essential. The new challenge is how to adapt an OF biosensor to detect multiple analytes. Multiparameter interferometric sensors have only recently attracted attention.[25] Just a few examples of multisensors have been reported for biomedical applications.[26] Most of them are focused on dual-parameter sensors of physical parameters (temperature and pH or pressure).[27] Only a few examples of double[28] or triple[29] detection exist, including biological material by interferometric fibers. For example, Xie et al. proposed a multiplexed fiber biosensor based on a dual Fabry-Perot-cavity. They detected the biotin-streptavidin interaction, including a negative control, thanks to the two independent cavities.[28] Li et al. combined a dual SPR-based sensing area and a Mach–Zender interferometer on an OF to detect the hybridization of the Epithelial Growth Factor Receptor gene, compensating the pH and temperature variations of the detection media.[29] This is an interesting approach to solving the problem of biosensor susceptibility to temperature and pH variation. However, in these studies, the sensing areas are along the fiber, and this configuration is not well adapted for localized and compact multiplex detection. An interesting and elegant alternative is the use of fiber assemblies or multicore fibers. Each multifiber assembly core can act as an independent waveguide and transfer a signal over a certain distance. Theoretically, if a transduction element is fabricated on these bundles, each core can be treated as an individual biosensor, which dramatically improves the compactness and integration of the sensor tip. A few attempts of multiplexed detection of biological targets have been made with such assemblies. Notably, Song et al. used a 500 µm fiber bundle containing 6000 individual fibers, each 3.1 µm in diameter, to construct a DNA array. This array was composed of microspheres, each functionalized with ODN. These were randomly immobilized at the tip of each fiber, which had been etched to form a microwell.[30] The device was used to detect several pathogens' ODN targets via fluorescence. Later, the same fiber bundle, modified to exhibit plasmonic properties, was used to remotely detect DNA hybridization.[31] Proof of multiplexed detection of two target molecules using the same kind of fiber bundle has been demonstrated by Desmet et al., where two areas of the bundle's tip were functionalized by rat IgG and one by rabbit IgG.[32] However, the fragility of the gold-coated microstructures would make it difficult to use this biosensor in a more rigid and complex environment. Concerning multicore interferometric devices, they are mainly used for monitoring physical parameters (strain, curvature, vibration, flow, torsion, RI) and have not yet been adapted for multiplexed biological detection.[33] Nevertheless, their ability to detect variations in the RI makes them good candidates for developing highly multiplexed biosensors while keeping their miniature structure, the number of probes being ideally only limited by the number of cores in the multi-fiber assemblies.

However, the functionalization with multiple probes of such a tiny surface at the tip of the OF assembly remains challenging. Automated microarrayers with a micrometer diameter stylus or ink-jet nozzle, currently used to deliver droplets of several hundred micrometers on planar substrates, lack the resolution to functionalize such small surfaces.[34,35] Methods based on dip-pen nano-lithography and using an Atomic Force Microscope tip to deliver receptors directly to microscale areas offer dramatically better resolution for droplet delivery but are not adapted to the geometry and size of OFs.[36] Recently, Courson et al. proposed a polymer cantilever realized by 3D stereolithography.[37] Several droplets were deposited at the tip of a nanostructured gold-coated OF assembly to demonstrate the ability to perform deposition on unconventional surfaces. Since the cantilever was made from a soft polymer, droplets were deposited via direct contact without damaging the patterned surface. However, this study only validated the possibility of depositing water/glycerol drops at the end

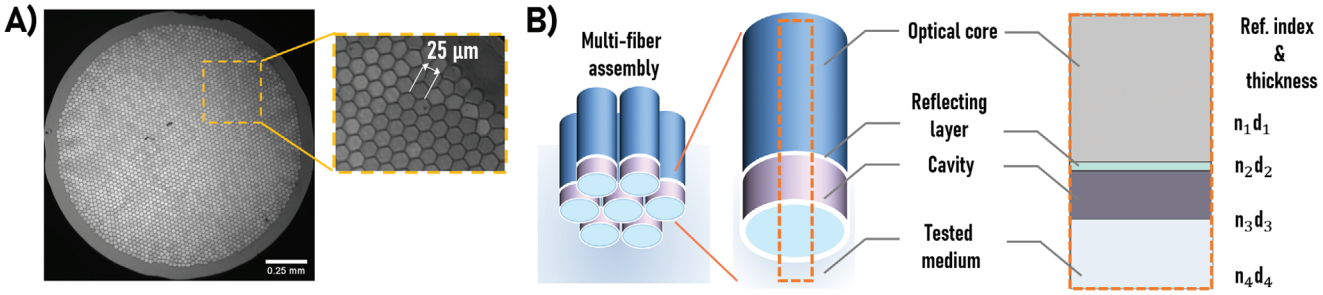

Figure 1. A) Optical image of IC and zoom on the individual cores. B) Schematic representation of one optical guide in the multicore assembly and corresponding equivalent model used for transducer study.

of an OF assembly. No biological probes were deposited, and no biodetection was performed on the fiber assembly.

In the present work, we have investigated the fabrication and the interferometric ability of a multicore waveguide consisting of 3012 cores. Two interferometric layers were deposited on the IC, a semi-reflecting tantalum pentoxide (Ta_2O_5) layer and a silicon dioxide (SiO_2) cavity, conferring interferometric properties to the device. The thicknesses of the deposited layers were estimated using a simulation of the interferometry phenomenon. Interferometric signals were remotely detected through the assembly itself, allowing us to measure its spectral response, sensitivity to RI variations, and resolution in the RIU. The coated surface of the waveguides was then fully silanized and locally functionalized with two single-stranded ODN probe arrays thanks to the previously mentioned polymer cantilever.[37] Finally, we revealed the full potential of the device by being able to monitor remotely the kinetics of ODN hybridization of the complementary strands while having negative control. We also demonstrated that each core of the assembly acts as an independent interferometric sensor by extracting the individual responses. This study prepares the ground for the future development of multiparametric diagnostic tools suitable for in vivo use.

2. Results and Discussion

2.1. Materials Choice and Sample Preparation

In the present work, we developed an interferometric transducer on a multicore assembly based on an IC composed of 3012 individual cores 25 µm in diameter (**Figure 1**A). Two layers were deposited at the top of the IC face: the internal semi-reflecting layer was made of Ta_2O_5 and the cavity was made of SiO_2 (Figure 1B). Both materials were used in the patented fiber-optic assay apparatus based on phase-shift interferometry.[38,39] The RI of Ta_2O_5 is equal to 2.10, whereas for SiO_2, it is 1.46 at $\lambda = 589.3$ nm.[40] RIs for both materials do not change significantly for the visible and beginning of the near-infrared regions, while the transmission of materials is high. Concerning the influence of temperature on material properties like layer thickness and RI change, the aforementioned materials are quite stable.[41–44] Regarding biocompatibility, several studies demonstrated that bulk Ta_2O_5 has cytocompatibility and anti-corrosive properties, allowing it to be used in potential medical devices.[45–48] The bulk form of SiO_2, widely used as a main material for fibers in biosensors based on OFs, also possesses cytocompatibility[49–51] and is compatible with the silanization process used for surface functionalization.[52]

Regarding interferences, the main role of the high-RI Ta_2O_5 layer is to increase the reflectivity since the RI contrast between the cavity layer of SiO_2 and the fiber material is low. When the targeted material binds to the surface, the cavity length increases, resulting in the interference pattern shifting toward longer wavelengths.[13] The thickness of the SiO_2 cavity influences the number and the position of maxima and minima obtained in the interferometric pattern. The Ta_2O_5 thickness mainly influences the contrast of the interferometric pattern and the quantity of retro-reflected light that can be collected.

Once the materials had been chosen, we entrusted the coating process to the Kerdry company.[53] Samples with different thickness combinations were produced by the ion-assisted electron beam evaporation technique. In this article, we present the results obtained on the most sensitive device with thicknesses ≈10 nm for Ta_2O_5 and 500 nm for SiO_2. To confirm the relevancy of this geometry and evaluate its performance, sensitivity to RI changes in the tested medium was investigated.

2.2. Optical Characterization

The characterization protocol and data treatment steps described in the materials and methods section were applied for the optical characterization of the IC.

2.2.1. Spectral Characterization

The spectral interrogation of the IC with interferometric layers was done using the setup depicted in Figure S1 (Supporting Information). Its calculated experimental sensitivity is given in **Figure 2**A. The obtained sensitivity curve presents peaks, nodes, and valleys corresponding to positive, null, and negative sensitivities. The theoretical sensitivity curve, obtained from the Finite Element Method (FEM) method (see materials and methods section), was superimposed on the experimental curve. An adaptation of the cavity thickness for a theoretical response was made to match the spectral position of the experimental sensitivity curve. For instance, a 9.5 nm semi-reflecting layer and a 532 nm cavity provided the closest spectral match with the experimental response. Despite the lack of smoothness of the experimental curve, its shape was in agreement with the theoretical

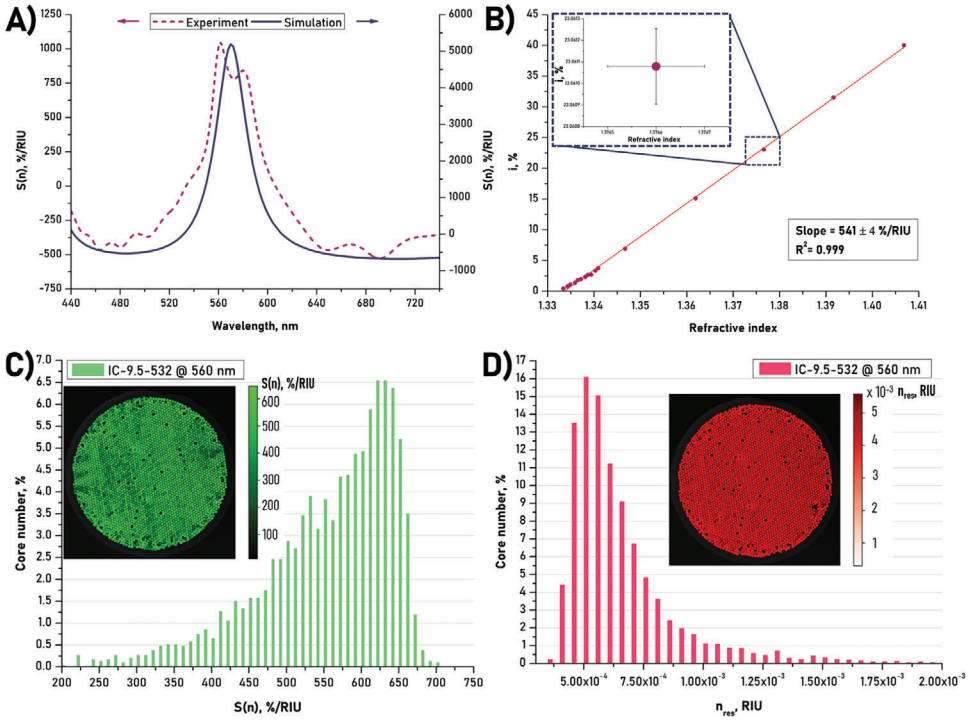

Figure 2. Optical characterization and comparison theory versus experiment. A) Experimental and optimized simulated spectral sensitivity. B) Normalized intensity of one core of the same IC interrogated at 560 nm with an upward intensity variation trend. C) Histogram for sensitivity and the corresponding color-coded map in the insert. D) Histogram for resolution and the corresponding color-coded map in the insert.

curve and allowed us to select the most optimal wavelength for intensity interrogation. For instance, a 560 nm excitation light could be used for intensity interrogation of this particular IC.

2.2.2. Intensity Characterization

The intensity interrogation of the IC was done at 560 nm using the setup depicted in Figure S2 (Supporting Information). The tested range of RI was between 1.332 and 1.401. The intensity signal was extracted from each core of the assembly from 20 independent images for each RI. Figure 2B shows the normalized intensity of the whole IC interrogated at 560 nm as a function of the RI. The sensitivity was estimated from the slope of this curve at 541 ± 4%.RIU^{-1}. Its positive value was in concordance with spectral interrogation while being below the estimated spectral sensitivity. This could be explained by the average over the whole bundles including the cladding. The experimental sensitivity of each core inside the IC was obtained similarly via intensity interrogation after core selection. The resolution of each core was subsequently calculated from the sensitivity and the maximum noise of the averaged normalized intensity signal, as described in the materials and methods part. Both data were presented as a color-coded map (see inserts in Figure 2C,D). These maps demonstrate the sensitivity and resolution of each core that could be extracted during core analysis. Due to their number, pitch, and sometimes irregular shape, some cores were not accessible and appeared as black spots. On the map, we can notice that none of the cores in the fiber bundle had the same responses. Sensitivity varied from 220 to 700%.RIU^{-1} and resolution from 1.9×10^{-3} to 3.5×10^{-4} RIU. To obtain a whole picture of IC individual core behavior and performance, the distribution of the core number in % with respect to the number of accessed cores in the IC as a function of corresponding sensitivities was created in the form of a bar chart (Figure 2C,D). The considered sample demonstrated a sensitivity with a distribution maximum of 630%.RIU^{-1}. 75% of cores possessed sensitivity better than 510%.RIU^{-1}. The resolution was represented in the same way. The studied sample had a distribution peak at 5.0×10^{-4} RIU while 75% of cores have better than 7.0×10^{-4} RIU. As sensitivities are not always given in the same units in the literature, the resolution is the only parameter that makes it possible to compare the performance of different developed biosensors. The best fiber-based interferometric devices, for both transmission and reflection modes, achieve resolutions of the order of 10^{-6} RIU.[54–57] The resolution obtained in our study may seem low compared to this. However, the reached value is sufficient for the detection of biomolecular interaction,[31,32] and above all, our device, unlike existing interferometric devices, comprises thousands of cores, giving it the capacity for multiplexed detection.

2.3. Surface Bio-Functionalization

The coated side of the waveguide assembly was used as a transducer platform to perform the biodetection assay. To consider any change of the tested medium non-related to the presence of a target molecule and/or to test the presence of several targets, different sensing areas have to be defined at the sensor surface. The multiplexed functionalization of the surface will permit the

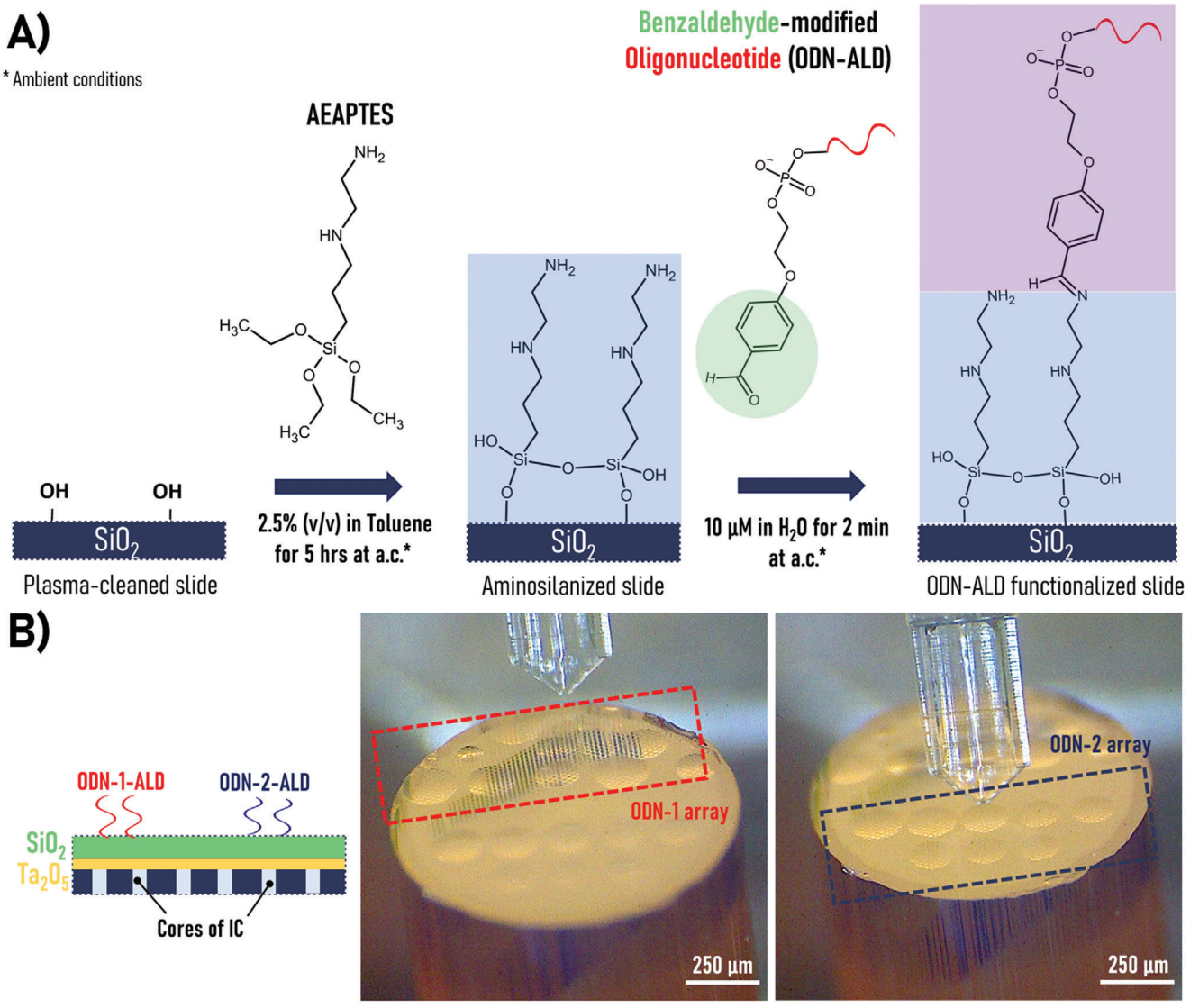

Figure 3. Principle of surface functionalization chemistry and arrays deposition. A) Surface functionalization principle based on AEAPTES and benzaldehyde-modified ODN, able to react directly with amino groups of deposited aminosilane. B) Deposited arrays of aldehyde-modified ODN on silanized IC with AEAPTES in the liquid phase with schematic representation of ODN-1-ALD and ODN-2-ALD arrays on the left and real view on the right.

concomitant detection of several biomarkers and the discrimination of the signal given by an unspecific phenomenon (unspecific surface interactions or bulk change of RI) from the specific target binding. Different aminosilanes were tested to immobilize multiple probe arrays on the coated surface of the assembly.[58] Our objective was to find chemistry requiring sufficiently short reaction times to prevent the drying of deposited spot-containing bioreceptors and giving adapted-sized droplets: allowing for spotting a few dozen drops on the whole surface of the optical bundle. Among the tested chemistries, the use of AEAPTES combined with benzaldehyde-modified probes was the most well-suited in terms of droplet size and reaction time (**Figure 3**A). Once the chemistry had been chosen, it was necessary to develop a deposition method adapted to the small surface of the IC tip. Microcontact deposition using newly developed 3D-printed polymeric microcantilevers proved to be the most suitable.[37] These cantilevers were soft enough to touch the IC apex without damage and to deposit microdroplets of solution with an appropriate size.

To demonstrate the proof of concept, two arrays of probes were deposited on the surface; two different benzaldehyde-modified ODN strands were used as probes: ODN-1-ALD and ODN-2-ALD. First, the SiO_2-coated waveguide assembly surface underwent silanization with AEAPTES in the liquid phase as described in the materials and methods section. The whole surface silanization was followed by localized spotting of 10 µM benzaldehyde-modified ODN solutions. The aldehyde group in the benzaldehyde-modified probe reacted with amino groups of aminosilane and formed a double carbon-nitrogen bond. A two-minute reaction was sufficient for proper probe grafting. The spotting solutions were prepared with 5% (v/v) glycerol to avoid

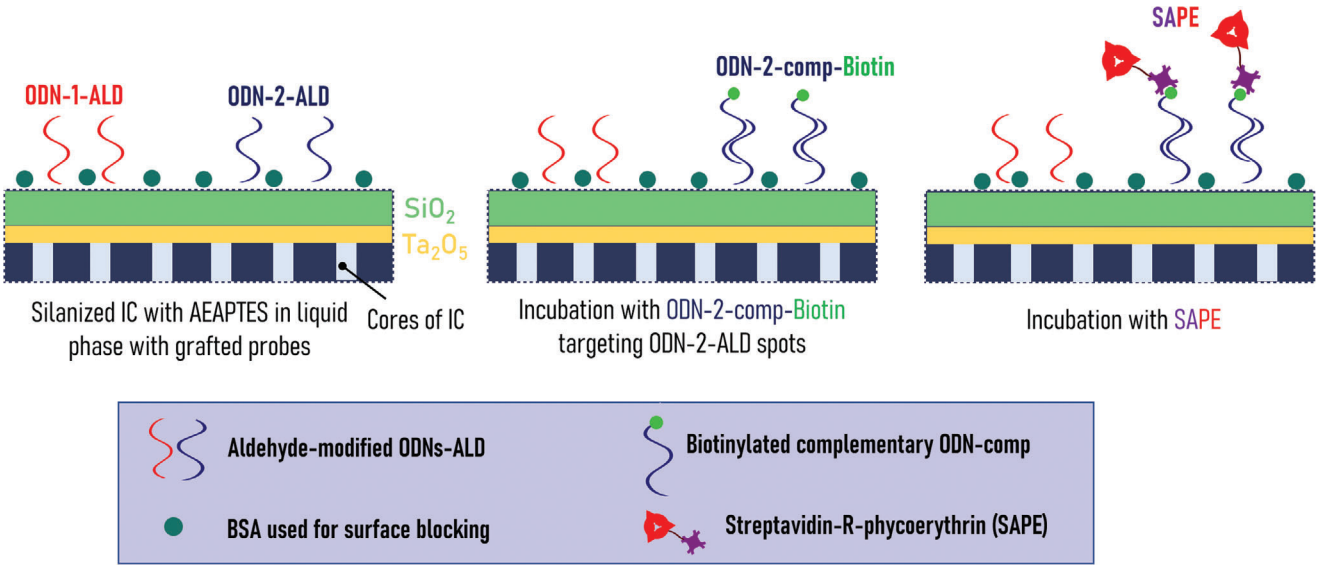

Figure 4. Multiplex biomolecular detection strategy. Schematic representation of incubation steps targeting ODN-2-ALD: from hybridization detection to fluorescence validation.

a complete spot drying. The spotting process was monitored in real-time with two cameras. The first allowed the control of the efficient droplet deposition, while the second controlled the level of the waveguide surface to prevent cantilever damage. The first array of ODN-1-ALD deposited on the top of the IC was formed by 11 droplets, whereas the second deposition containing ODN-2-ALD was made of 8 droplets (Figure 3B). Each microdroplet was in the order of hundred-micrometer size, covering an area of ≈50 to 60 cores (roughly corresponding to 3×10^4 μm^2 coated area, or ≈1/30 of the total surface).

2.4. Multiplexed Biodetection Assays

To demonstrate the feasibility of a multiplexed detection by interferometry on the functionalized IC and to validate it by fluorescence observation, the complementary strand of ODN-2-ALD, ODN-2-comp, labeled with biotin, was used as a target. Previously to the bioassay, the IC with grafted ODN-1-ALD and ODN-2-ALD was hydrated and blocked with BSA to reduce unspecific biomolecule binding. The target molecule was then incubated on the multifunctionalized surface of the IC. At ambient conditions, the hybridization step lasted 30 min, followed by RB rinsing. As fluorescence observation was used as an alternative analytical method to confirm the functionalization of the IC, the specific immobilization, and the detection of ODN-2, the last step was to incubate SAPE, a fluorophore, for 10 min, after which the unbound molecules were removed by rinsing several times with RB. The global strategy of the biosensing assay is summed up in **Figure 4**.

The retro-reflected light of the whole assembly was monitored in real-time from the injection of ODN-2-comp as described in the materials and methods. The variation of signals was monitored from two different areas on the IC surface selected between the two deposited arrays, ODN-1-ALD, and ODN-2-ALD spotted areas. The localization of functionalized areas was obtained through the differential image, where the first image from an image stack for a given injection was subtracted from all recorded images in this stack (**Figure 5** insert in A). The normalized intensities $i(t)$ of the aforementioned areas were obtained by the normalization procedure described in the materials and methods section. The signal analysis results on the two areas are shown in Figure 5A. An individual core signal extraction is presented in Figure 5B for 5 cores from ODN-1-ALD and ODN-2-ALD spotted areas.

The signal from the ODN-2-ALD area, functionalized with the probe complementary to the injected target ODN-2-comp, the positive control, steeply increased up to 1.15% after 600 s, where it changed to a gradual variation tendency reaching 1.5% (Figure 5A). The intensity of the ODN-1-ALD area, the negative control, varied around zero level during the whole detection. These results showed that, as expected, a biomolecular interaction occurred between ODN-2 and its complementary strand and that the detection was specific as the positive and negative control signals were well separated. The degree of signal variation of positive controls could be affected by many parameters like the quality of surface silanization, the density of deposited probes, the efficiency of certain ODN-ALD to recognize and bind complementary strands of ODN-comp, and the sensitivity of cores that contributed to the overall signal in selected areas. To study the influence of the latest, we extracted the signal of several individual cores, excluding the signal from cladding, within assigned areas for ODN-1-ALD and ODN-2-ALD. Five responses of individual cores from the ODN-1-ALD and ODN-2-ALD areas were compared. After the injection of ODN-2-comp, the signal variations of the individual cores from the ODN-2-ALD area had heterogeneous intensity profiles. Their plateaus varied from 1.0% to 2.1% compared to 1.5% of normalized intensity in zone-type selection (Figure 5B). This demonstrated the heterogeneity of cores' responses caused by the difference in sensitivity, which gave the mean response considering the cladding signal that reached the maximum of 1.5% in the zone-type observation. The level of

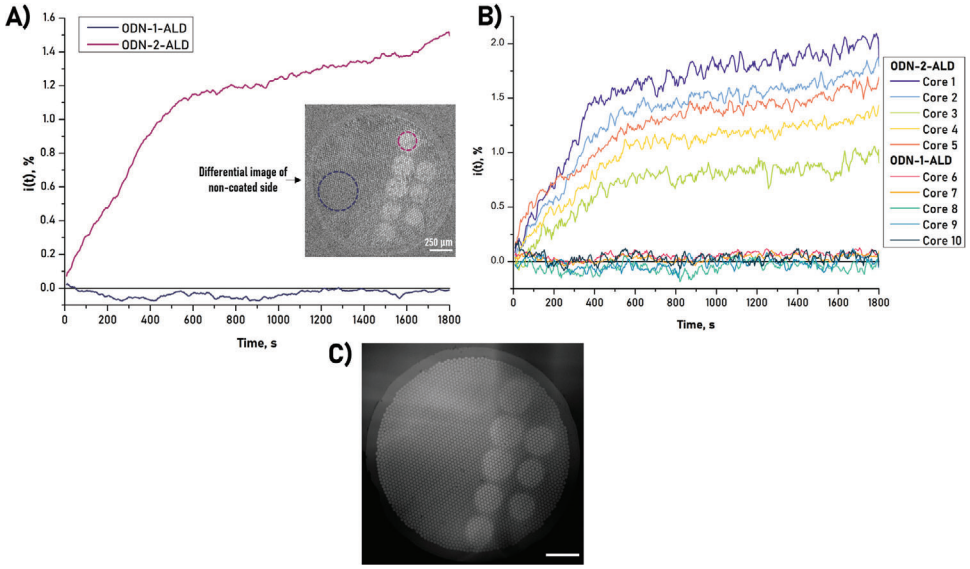

Figure 5. Biomolecular detection. A) Signal variation (with applied 5 points rolling average) extracted from ODN-1-ALD, ODN-2-ALD. Insert differential image observed after ODN-2-comp injection and areas selected for signal extraction. B) Evolution of signal (with applied 5 points rolling average) after injection of ODN-2-comp for 5 individual cores in ODN-1 and ODN-2 spotted areas. C) Fluorescence validation: fluorescence spots observed through the non-functionalized side of IC after SAPE injection.

noise in the curves was affected by the much smaller number of pixels for the selected cores than the area-type observation. The signals from individual cores from the ODN-1-ALD area, negative control, were hardly distinguishable from zero.

Once the detection experiment was finished, SAPE, a fluorescent dye that could bind to biotinylated complementary ODN-comp, was incubated on the sensing surface to validate the specific detection not only by interferometry but also by fluorescence. The LED, reflecting-unit mirror, and band-pass filter were replaced for fluorescence observation, as described in the materials and methods section. The contrasted image clearly shows that, as expected, the SAPE bound only to ODN-2-ALD spots since ODN-1-ALD were not bound to complementary strands. This alternative approach confirmed the specific biomolecular interaction at the surface of the assembly and demonstrated the preservation of ODN functionality after arraying on the spotted IC (Figure 5C).

The same steps were implemented with ODN-1-comp, the target complementary to ODN-1. We were not able to directly detect the hybridization of the complementary strand. This may be due to a low density of deposited probes caused by a less efficient grafting of ODN-1-ALD compared to ODN-2-ALD and/or to an unspecific interaction between ODN1-comp and ODN2-ALD, leading to a less visible hybridization detection. However, to amplify the signal and detect ODN-1-comp associated with their probes, we performed streptavidin injection. This experiment confirmed the presence of ODN-1-ALD and its specific biomolecular interaction with its complementary strand (Figure S8, Supporting Information).

3. Conclusion

In this study, we have presented the preparation, optical characterization, multiplexed functionalization, and biosensing validation of the interferometric IC composed of 3012 cores. The spectral characterization of the IC allowed us to estimate the thicknesses of deposited interferometric layers (the 9.5 nm semi-reflecting Ta_2O_5 layer and the 532 nm SiO_2 cavity) and to select an optimal wavelength for intensity interrogation. The optical characterization, performed at 560 nm, on individual cores demonstrated sensitivity and resolution distributions, with 75% of cores having sensitivity better than 510%. RIU^{-1} and resolution better than 7.0×10^{-4} RIU. The IC was locally functionalized with two arrays of DNA probes. The functionalization was based on ODN-ALD and AEAPTES chemistry combined with the use of a soft polymeric cantilever. This association provided two arrays of dozens of hundred-micrometer-size spots. A functionalized optical biosensor was then used as an optical platform to validate the proof of concept of a multiplexed, remote, label-free detection of complementary ODN strands. The biomolecule detection was monitored by imaging the non-functionalized end of the waveguide assembly. The un-spotted and the ODN-1-ALD spotted areas were used as negative control areas. The resulting unspecific signals were compared to those recorded on the ODN-2 spots, which confirmed the specific detection of ODN-2-comp hybridization in area-type and individual core areas. Fluorescence observation was used as an alternative analytical method to confirm this target's specific localization and detection. The multiplexed functionalization allowed us to define negative control areas that could be used to sense any global change at the surface due to temperature, global RI variations, or unspecific surface interactions. This ability is necessary for the future use of the device in complex media since the RI of the environment can vary without being correlated to the presence of targeted molecules. The demonstrated potential of the biosensor to perform a detection including positive and negative controls and its intrinsic ability to be used in specific micro-environments open the way toward in situ diagnostics. Indeed, multiplexed detection is required for

Table 1. Composition of RB and HB.

RB	PBS 0.01 M, NaCl 0.537 M, KCl 2.7 mM, 0.15% (v/v) Tween
HB	PBS 0.01 M, NaCl 0.537 M, KCl 2.7 mM, 0.05% (v/v) Tween, Denhardt 25x, salmon DNA 5 mg/mL

applications in complex media to take into account unspecific contributions and also to have several parameters analyzed on a single device to establish a reliable diagnosis. To get closer to medical applications, the next steps will be to develop the same strategy for flexible OFs having a few hundred microns in diameter, increasing the number of probes and the diagnostic relevance of targets, carrying out concentration ranges to determine detection limits and performing detections in more complex media to effectively test the biosensor's specificity.

4. Experimental Section

Reagents: Phosphate Buffer Saline (PBS), NaCl, KCl, $CaSO_4$, Bovine Serum Albumin (BSA), Tween20, anhydrous Toluene, anhydrous Ethanol, 98% Acetone, Denhardt's Solution, Salmon sperm DNA, and glycerol were purchased from Sigma Aldrich (Saint Quentin Fallavier, France). Fluorescence was validated with Streptavidin-Phycoerythrin (SAPE) from Fisher Scientific (Illkirch, France). Streptavidin, used for signal amplification, was also purchased from Fisher Scientific (Illkirch, France). N-(2-Aminoethyl)-3-aminopropyltriethoxysilane (AEAPTES) was purchased from Gelest Inc. (Frankfurt am Main, Germany). 96% pure Ethanol was purchased from Carlo Erba reagents (Val de Reuil, France).

The composition of the Rinsing Buffer (RB) and the Hybridization Buffer (HB) are given in **Table 1**.

ODN strands were purchased from Eurogentec (Seraing, Liège, Belgium) and had the following sequences and chemical modifications (ALD for aldehyde, Biot for biotin) (**Table 2**).

Optical Waveguide Preparation: ICs with a diameter of 1.6 mm comprising 3012 individual cores 25 µm in diameter (38-305, Edmund Optics) were used to fabricate the interferometric biosensor assembly. The ICs were entrusted to the Kerdry company,[53] which coated them with two layers (TaO_2 and SiO_2) to give them interferometric properties. Kerdry used the ion-assisted electron beam evaporation technique, which involves evaporating target material with an electron gun and bombarding the evaporated atoms with ions from an ion source.[59] The mixed flux of target atoms and ions arrives on the sample fixed on a rotating substrate, allowing for low-temperature film deposition. Kerdry used Balzers BAK 600 coating machine, where the purity of the used target material for Ta_2O_5 and SiO_2 was 99.99%. The deposition of the two films was consecutive without breaking the vacuum. The base vacuum in the chamber was 3×10^{-6} mbar, while the working pressure during the deposition was 2×10^{-4} mbar. The deposition temperature was in the range of [60–80] °C. The acceleration voltage of the e-gun was 10 kV. The ion gun had a Kaufman configuration, where Ar^+ ions were used for bombardment. The substrate with samples bombarded by target atoms and ions rotated at 37 rpm. To produce the oxide, O_2 was introduced into the chamber. The deposition rate of Ta_2O_5 and SiO_2 film was in the range of [0.2–0.6] nm s^{-1}. A quartz microbalance was used to stop deposition once it reached the required thickness. The indicated precision of quartz microbalance was ±5% of the measured thickness. A 2 mm thick BK7 substrate, a witness sample, was introduced as an alternative approach to estimate the thickness of deposited films.

Table 2. Sequences of ODN probes and complementary targets.

Name of sequence	Sequence 5′ → 3′ (Modification at 5′)
ODN-1-ALD	ALD-TTT-TTT-TTT-TGA-CCG-GTA-TGC-GAC-CTG-GTA-TGC-G
ODN-2-ALD	ALD-TTT-TTT-TTT-TGA-CCA-TCG-TGC-GGG-TAG-GTA-GAC-C
ODN-1-comp biotin	Biot-CG-CAT-ACC-AGG-TCG-CAT-ACC-GGT-C
ODN-2-comp biotin	Biot-GG-TCT-ACC-TAC-CCG-CAC-GAT-GGT-C

Optical Characterization—Optical Setup(s): An optical setup equipped with exchangeable light sources (a white light source (Thorlabs, SLS201L(/M)), a 565 nm (Thorlabs, M565F3), and a 490 nm LED source (Thorlabs, M490F2)), a 560 nm (Thorlabs, FBH560-10) and a 578 band-pass filters (Thorlabs, FBH580-10), a spectrophotometer (Thorlabs, CCS100/M) or a CMOS Camera (C11440, Orca-flash4.0LT, Hamamatsu) was conceived to collect, image, and quantify the retro-reflected light coming back from the sensitive surface of IC (see Figures S1 and S2, Supporting Information). This setup allowed both the spectral and intensity characterizations of the assembly, giving access to sensitivities and resolutions of the different cores composing the assembly. It also permitted to follow through the interferometric phenomenon any further modification of RI and/or thickness of bound targets occurring within the sensitive areas of the surface. The retro-reflected intensity could be measured in real-time on every core composing the assembly. The same setup was used for the fluorescence revelation of bound targets by changing the illuminating LED from 565 to 490 nm, the semi-reflecting mirror to a dichroic mirror, and the band-pass filter from 560 to 578 nm as illustrated in the Supporting Information optical setup part and in Figure S3 (Supporting Information).

Protocol and Data Treatment for Sensitivity and Resolution Determination: Before any further modification or use of the system as a biosensor, the global sensitivity of the assembly to RI changes was characterized. The coated side of the assembly was placed successively into solutions of known RI from 1.332 (water) to 1.401 (50% (v/v) water/glycerol solution), and several spectra or images were registered. The RI was measured using a Hanna instrument HI 96 801 refractometer with 10^{-4} RIU resolution (0.1% brix).

The retro-reflected intensity $I(n)$ was measured at different RI n on the whole assembly as a function of wavelength for the spectral characterization and on different areas (or individual cores) as a function of image number for the intensity characterization. $i(n)$, the relative normalized retro-reflected intensity, was defined as follows:

$$i\ (n) = \frac{I\ (n) - I_{ref}}{I_{ref}} \tag{1}$$

where I_{ref} represents the retro-reflected intensity in water.

The sensitivity was quantified from $i(n)$ as:

$$S = \frac{di}{dn} \tag{2}$$

The resolution R, was determined from the intensity characterization, taking σ, the maximum noise of normalized intensity, and S, then:

$$R = \frac{3\sigma}{S} \tag{3}$$

The detailed data treatment is described in paragraph S.2 of the Supporting Information and Figures S4 and S5 (Supporting Information).

Calculation of the Theoretical Sensitivity: In our study, the wave optics module of COMSOL Multiphysics software (version 5.5) was employed, utilizing the FEM to simulate the resolution and transmittance of light within a specific wavelength range through a designed OF sensor geometry. This simulation was simplified by considering a planar wave and representing the sensor geometry in two dimensions, focusing on a section of the optical core. This section excluded the fiber cladding but included a reflective layer, a cavity, and the medium under test. Each section of the

model was assigned specific values of RI (real part), and thickness with RI dispersion (except the tested medium), accounted for at the tested light wavelength.

The simulation was governed by the wave equation for the electric field component in a non-conductive, source-free medium ($\sigma = 0$), expressed as:

$$\nabla \times \left(\nabla \times \vec{E} \right) - k_0^2 n^2 \vec{E} = 0 \tag{4}$$

here, $\vec{E}(x, y, z) = \vec{E}(x, y) \exp(-ik_z \cdot z)$, with $k_0 = 2\pi/\lambda$ representing the free space wave number, λ wavelength of excitation light wave, n the RI of the material for each model section, and k_z and z denoting the out-of-plane wave number and coordinate, respectively.

To model wave propagation accurately, two periodic boundary conditions were applied along the left and right edges of the model, perpendicular to the wave's direction of travel. The wave propagation was initiated within the core itself. By altering both the excitation wavelength and the RI of the medium under test, a theoretical spectral response was generated, depicting reflectance as a function of wavelength for various RIs. The model's theoretical sensitivity was derived using a methodology akin to experimental spectral analysis, which involved signal normalization and subsequent sensitivity estimation.

Multiplex Surface Biofunctionalization: The IC, previously optically characterized, was submitted to plasma cleaning using a Diener electronic Femto low-pressure plasma system (3 min, 75% O_2, 25% Ar, 0.6 mbar pressure, 80% generator power). It was then silanized with AEAPTES in the liquid phase. For this, its coated end face with interferometric layers was submerged in 2.5% (v/v) AEAPTES solution prepared in anhydrous Toluene. The reaction occurred inside a desiccator with $CaSO_4$ desiccant anhydrous (stored at 110 °C before use) to absorb any excess water in the environment and prevent the potentially uncontrolled polymerization of silane molecules. The desiccator was sealed with silicon grease and left to react for 5 h at ambient temperature under a fume hood. Afterward, to remove unbound AEAPTES molecules, a series of consecutive two-minute baths with anhydrous toluene, anhydrous ethanol, ethanol (96% pure), and deionized water (DI, 18 MΩ•cm was performed under agitation. The rinsed sample was then dried with Argon and placed inside a furnace for 1 h at 110 °C. The curing step finalized the silanization, where excess water molecules evaporated, forming a siloxane (Si—O) bond with the substrate.

A polymeric microcantilever (referred to as V1 in)[37] made of DS-3000 biocompatible photoresist (DWS, Italy) with a special geometry was fabricated by stereolithography (Dilase 3D, Kloe SA) according to previous work.[37] The device was used to deposit microdrops of solutions on the previously silanized face of the assembly. The cantilever was installed in a spotting system containing x–y–z linear motorized stages (UTS-100CC, Newport) with a 0.3 µm minimum motion step, a motion controller (ESP301, Newport), and a CMOS camera (DigiMicro 2.0 Scale, Toolcraft, Conrad) for visual control placed on the stages. An extra camera (DigiMicro 2.0 Scale, Toolcraft, Conrad) was placed separately on an optical table perpendicularly to the stages for visual control in the perpendicular direction. The assembled system was monitored by a custom-built Labview software dedicated to controlling stage position, speed, spotting time, map programming, live visual control, and image recording (see Figure S6, Supporting Information for an overview of the spotting system).

Before the spotting, the first-time used cantilever underwent several short treatments with low-power (10%) Oxygen plasma to improve its wettability. It was then rinsed with DI water, ethanol, and DI water again and dried in the air. The solutions used for spotting containing 10 µM of aldehyde-modified, shortly ODN-ALD, and 5% (v/v) of glycerol were placed in loading wells. The spotting map for each array of ODN on the assembly surface and the position of wells with spotting solutions were recorded using Labview. To avoid damaging the cantilever and successfully depositing droplets, the IC surface level was monitored using the extra camera. The first probe solution was loaded on the microcantilever by immersion in loading wells, and the first array of ODN-1-ALD was deposited on the silanized face of the IC. The cantilever was copiously rinsed with DI water, ethanol, and DI water before the deposition of the second array of ODN-2-ALD to prevent contamination. After all arrays were finished, the probes were left to react with the surface for at least 2 min. The whole IC surface was then rinsed by immersion in DI water, dried with Argon, and stored at 4 °C before being used for biosensing assay.

Multiplexed Biodetection Assays: To detect biomolecular interactions, the same setup used during the intensity interrogation of IC was used (Figure S2, Supporting Information). The room temperature was kept constant at ≈25 ± 1 °C while the light sources and camera were left to stabilize for at least 1 h before the biosensing experiment. A dedicated reservoir was developed to immerse IC in tested solutions (Figure S7, Supporting Information). The reservoir was prepared from a mixture of Polydimethylsiloxane (PDMS) (184 silicone elastomer base (90% w/w) and silicone elastomer curing agent (10% w/w) from Sylgard 184) and carbon powder in a 1:4 weight proportion and poured into a small plastic Petri dish containing a piece of tube that played the role of mold. Afterward, the sample was degassed and left in a furnace at 100 °C for several hours until it was solidified. The carbon powder was used to make the fabricated support capable of absorbing the light emerging from the IC to minimize the reflected light that could influence measurements on the IC. The shape and materials were chosen to reduce the quantity and the loss of used products: small volume, low biomolecule adsorption surface properties.

The functionalized tip of IC was inserted inside the channel formed by mold inside the solidified PDMS. The small dimension and flexibility of the material allowed a relatively tight joint between the sample and the support.

The functionalized side was hydrated by immersion in DI water for 5 min. It was then immersed in RB for 5 min and in the solution of PBS containing 1% (w/v) BSA to block unfunctionalized areas and prevent non-specific adsorption at the latter stage. The excess of BSA was gently rinsed with RB.

The sensing solutions were injected by a conventional laboratory pipette while the liquid was evacuated by a syringe attached to a long blunt needle (Figure S7, Supporting Information).

The target solution composed of 0.2 µM complementary biotinylated ODN-2-comp prepared in HB was incubated for ≈30 min at ambient temperature to reach signal stabilization before rinsing three times with RB. The interferometric signal was monitored with the optical system during the whole experiment by measuring the retro-reflected light intensity $I(t)$ on the different localized functionalized areas (or on individual cores) as a function of time. The recording was stopped for rinsing and solution replacement. The initial signal on each area, at the beginning of the recording t_0, was reduced to zero by subtraction of the mean intensity on the area at t_0, $I(t_0)$. The exploited normalized signal $i(t)$ is finally given by:

$$i\ (t) = \frac{I\ (t) - I\ (t_0)}{I\ (t_0)} \tag{5}$$

To confirm the multiplexed biodetection observed by interferometry via an independent method, biotinylated ODN-comp targets were used and revealed fluorescence after subsequent incubation in SAPE (5% (v/v) in RB) for 10 min and rinsing with RB to remove unbounded molecules. Fluorescence images of the reactive face of the assembly were acquired using the same optical setup with the modifications mentioned in paragraph Figure S1 (Supporting Information).

To test the biosensing by the second grafted probe, the target solution composed of 0.2 µM complementary biotinylated ODN-1-comp prepared in HB was introduced to PDMS support. The solution was incubated for ≈30 min to reach signal stabilization before rinsing three times with RB. To increase the strength of the interferometric signal, streptavidin (1 µM in PBS) was incubated for 10 min and rinsed with RB to remove unbounded molecules. As previously described, the interferometric signal was monitored with the optical system during the experiment.

All detection steps were performed in darkness to avoid the influence of ambient light.

Supporting Information

Supporting Information is available from the Wiley Online Library or from the author.

Acknowledgements

This project has received financial support from the CNRS through the MITI interdisciplinary programs through its exploratory research program and from Grenoble Alpes University through the IRS and IRGA exploratory and emerging research programs. The Ph.D. of O. Bratash was funded by the CEA (PHARE Ph.D.). SyMMES laboratory is part of Labex LANEF, Labex ARCANE, and CBH-EUR-GS (ANR-17-EURE-0003). This work was supported by the European Union's Horizon 2020 research and innovation program as part of the HoliFAB project (grant agreement no. 760927), by the FEDER European Regional Funds and French Région Occitanie as part of the MultiFAB project (grant agreement number 16007407/MP00115MP0011594), and by the French national technological network RENATECH.

Conflict of Interest

The authors declare no conflict of interest.

Data Availability Statement

The data that support the findings of this study are available from the corresponding author upon reasonable request.

Keywords

biosensor, image conduit, interferometry, multiplex, optical waveguide assembly, remote bio-detection

Received: November 26, 2024
Published online:

[1] A. Klein, T. Fell, C. Birkenmaier, J. Fromm, V. Jansson, T. Knösel, H. R. Dürr, *Cancers* **2021**, *13*, 1393.
[2] I. C. Bennett, A. Saboo, *World J. Surg.* **2019**, *43*, 1054.
[3] A. Bex, B. Mathon, *Neurosurgical Review* **2022**, *46*, 5.
[4] F. Ferrara, S. Zoupanou, E. Primiceri, Z. Ali, M. S. Chiriacò, *Biosens. Bioelectron.* **2022**, *196*, 113698.
[5] M. M. J. Bauman, S. M. Bouchal, D. D. Monie, A. Aibaidula, R. Singh, I. F. Parney, *Neurosurgical Focus* **2022**, *53*, E14.
[6] R. Sadeh, I. Sharkia, G. Fialkoff, A. Rahat, J. Gutin, A. Chappleboim, M. Nitzan, I. Fox-Fisher, D. Neiman, G. Meler, Z. Kamari, D. Yaish, T. Peretz, A. Hubert, J. E. Cohen, A. Salah, M. Temper, A. Grinshpun, M. Maoz, S. Abu-Gazala, A. Ben Ya'acov, E. Shteyer, R. Safadi, T. Kaplan, R. Shemer, D. Planer, E. Galun, B. Glaser, A. Zick, Y. Dor, et al., *Nat. Biotechnol.* **2021**, *39*, 586.
[7] L. Hamard, D. Ratel, L. Selek, F. Berger, B. van der Sanden, D. Wion, *J. Neuro-Oncol.* **2016**, *128*, 1.
[8] W. Liu, Z. Liu, Y. Zhang, S. Li, Y. Zhang, X. Yang, J. Zhang, L. Yuan, *Opt. Laser Technol.* **2022**, *152*, 108167.
[9] L. Zu, X. Wang, P. Liu, J. Xie, X. Zhang, W. Liu, Z. Li, S. Zhang, K. Li, A. Giannetti, W. Bi, F. Chiavaioli, L. Shi, T. Guo, *Adv. Sci.* **2024**, *11*, 2308783.
[10] F. Chiavaioli, D. Janner, *J. Lightwave Technol.* **2021**, *39*, 3855.
[11] F. Chiavaioli, D. Santano Rivero, I. Del Villar, A. B. Socorro-Leránoz, X. Zhang, K. Li, E. Santamaría, J. Fernández-Irigoyen, F. Baldini, D. L. A. van den Hove, L. Shi, W. Bi, T. Guo, A. Giannetti, I. R. Matias, *Adv. Photonics Res.* **2022**, *3*, 2200044.
[12] X. Li, N. Chen, X. Zhou, P. Gong, S. Wang, Y. Zhang, Y. Zhao, *Journal of Biophotonics* **2021**, *14*, 202100068.
[13] D. Burnat, M. Janik, N. Kwietniewski, A. Martychowiec, P. Musolf, K. Bartnik, M. Koba, T. P. Rygiel, J. Niedziółka-Jönsson, M. Śmietana, *Sci. Rep.* **2024**, *14*, 23127.
[14] O. Bratash, A. Buhot, L. Leroy, E. Engel, *Biosens. Bioelectron.* **2024**, 116088.
[15] B. Li, R. Zhang, R. Bi, M. Olivo, *Biosensors* **2023**, *13*, 64.
[16] Y. R. Wang, Z. Q. Tou, R. Ravikumar, Y. Y. Lim, Z. W. Ding, C. L. Zhao, P. L. So, C. C. Chan, *J. Lightwave Technol.* **2019**, *37*, 2773.
[17] K. Wysokiński, D. Budnicki, J. Fidelus, Ł. Szostkiewicz, Ł. Ostrowski, M. Murawski, M. Staniszewski, M. Staniszewska, M. Napierała, T. Nasiłowski, *Biosens. Bioelectron.* **2018**, *114*, 22.
[18] R. Wang, M. Yan, M. Jiang, Y. Li, X. Kang, M. Hu, B. Liu, Z. He, D. Kong, *Anal. Chim. Acta* **2023**, *1252*, 341051.
[19] S. Tang, M. Zou, C. Zhao, Y. Jiang, R. Chen, Z. Xu, C. Yang, X. Wang, B. Dong, Y. Wang, C. Liao, G. Xu, *Biosensors* **2022**, *12*, 391.
[20] "Protein Analysis" can be found under, https://www.sartorius.com/en/products/protein-analysis (accessed: July 2024).
[21] I. Ziu, E. T. Laryea, F. Alashkar, C. G. Wu, S. Martic, *Anal. Bioanal. Chem.* **2020**, *412*, 1193.
[22] H. Zhang, W. Li, H. Luo, G. Xiong, Y. Yu, *Chem.-Biol. Interact.* **2017**, *276*, 141.
[23] D. Seo, S.-H. Paek, S. Oh, S. Seo, S.-H. Paek, *Sensors* **2016**, *16*, 1581.
[24] S. Gao, B. Hu, X. Zheng, Y. Cao, D. Liu, M. Sun, B. Jiao, L. Wang, *Biosens. Bioelectron.* **2016**, *79*, 938.
[25] S. Pevec, D. Donlagić, *Optical Engineering* **2019**, *58*, 072009.
[26] R. Correia, S. James, S.-W. Lee, S. P. Morgan, S. Korposh, *J. Opt.* **2018**, *20*, 073003.
[27] G. A. Lashari, F. Mumtaz, Z. Ai, Y. Dai, *Optik* **2023**, *282*, 170860.
[28] L. Xie, L. V. Nguyen, H. Ebendorff-Heidepriem, S. Warren-Smith, *IEEE Sens. J.* **2019**, *19*, 10425.
[29] X. Li, P. Gong, X. Zhou, S. Wang, Y. Liu, Y. Zhang, L. V. Nguyen, S. C. Warren-Smith, Y. Zhao, *Anal. Chim. Acta* **2023**, *1263*, 341286.
[30] L. Song, S. Ahn, D. R. Walt, *Anal. Chem.* **2006**, *78*, 1023.
[31] K. Vindas, L. Leroy, P. Garrigue, S. Voci, T. Livache, S. Arbault, N. Sojic, A. Buhot, E. Engel, *Anal. Bioanal. Chem.* **2019**, *411*, 2249.
[32] C. Desmet, K. Vindas, R. A. Meza, P. Garrigue, S. Voci, N. Sojic, A. Maziz, R. Courson, L. Malaquin, T. Leichle, A. Buhot, Y. Roupioz, L. Leroy, E. Engel, *Sensors* **2020**, *20*, 511.
[33] Y. Yao, Z. Zhao, M. Tang, *Sensors* **2023**, *23*, 3436.
[34] S. Brenet, A. John-Herpin, F.-X. Gallat, B. Musnier, A. Buhot, C. Herrier, T. Rousselle, T. Livache, Y. Hou, *Anal. Chem.* **2018**, *90*, 9879.
[35] L. O'Connell, O. Mandula, L. Leroy, A. Aubert, P. R. Marcoux, Y. Roupioz, *Chemosensors* **2022**, *10*, 192.
[36] P. Dey, N. Fabri-Faja, O. Calvo-Lozano, R. A. Terborg, A. Belushkin, F. Yesilkoy, A. Fàbrega, J. C. Ruiz-Rodriguez, R. Ferrer, J. J. González-López, M. C. Estévez, H. Altug, V. Pruneri, L. M. Lechuga, *ACS Sens.* **2019**, *4*, 52.
[37] R. Courson, O. Bratash, A. Maziz, C. Desmet, R. A. Meza, L. Leroy, E. Engel, A. Buhot, L. Malaquin, T. Leïchlé, *Microsyst. Nanoeng.* **2023**, *9*, 85.
[38] H. Tan, Y. Tan, D. J. Chen, K. L. Witte, *Fiber-Optic Assay Apparatus Based on Phase-Shift Interferometry* **2005**, WO2005047854A2.
[39] A. Jug, T. Bratkovič, J. Ilaš, *TrAC, Trends Anal. Chem.* **2024**, *176*, 117741.
[40] L. V. Rodríguez-de Marcos, J. I. Larruquert, J. A. Méndez, J. A. Aznárez, *Opt. Mater. Express* **2016**, *6*, 3622.
[41] W. Souder, P. Hidnert, *SCI. PA. NATL. BUR. STAND.* **1925**, *21*, 1.

[42] D. B. Leviton, B. J. Frey, *InOptomechanical Technologies for Astronomy* **2006**, *62732K*, 800.
[43] C.-L. Tien, C.-C. Lee, K.-P. Chuang, C.-C. Jaing, *J. Mod. Opt.* **2000**, *47*, 1681.
[44] A. K. Chu, H. C. Lin, W. H. Cheng, *J. Electron. Mater.* **1997**, *26*, 889.
[45] T. Ruckh, J. R. Porter, N. K. Allam, X. Feng, C. A. Grimes, K. C. Popat, *Nanotechnology* **2008**, *20*, 045102.
[46] H.-L. Huang, Y.-Y. Chang, H.-J. Chen, Y.-K. Chou, C.-H. Lai, M. Y. C. Chen, *Journal of Vacuum Science & Technology A* **2014**, *32*, 02B117.
[47] T. Beline, A. B. de Almeida, N. F. Azevedo Neto, A. O. Matos, A. P. Ricomini-Filho, C. Sukotjo, P. J. M. Smeets, J. H. D. da Silva, F. H. Nociti, V. A. R. Barão, *Appl. Surf. Sci.* **2020**, *520*, 146326.
[48] S. T. Rajan, M. Das, A. Arockiarajan, *J. Alloys Compd.* **2022**, *905*, 164272.
[49] D. Sahu, G. M. Kannan, M. Tailang, R. Vijayaraghavan, *Journal of Nanoscience* **2016**, *2016*, 4023852.
[50] A. Katsumiti, I. Arostegui, M. Oron, D. Gilliland, E. Valsami-Jones, M. P. Cajaraville, *Nanotoxicology* **2016**, *10*, 185.
[51] G. Voskerician, M. S. Shive, R. S. Shawgo, H. von Recum, J. M. Anderson, M. J. Cima, R. Langer, *Biomaterials* **2003**, *24*, 1959.
[52] N. Dendane, A. Hoang, L. Guillard, E. Defrancq, F. Vinet, P. Dumy, *Bioconjugate Chem.* **2007**, *18*, 671.
[53] "Réalisation de traitements optiques, antireflets, filtres, Back Coating, miroir", can be found under, https://kerdry.com/traitement-optique/ (accessed: July 2024).
[54] X. Li, Y. Shao, Y. Yu, Y. Zhang, S. Wei, *Sensors* **2016**, *16*, 794.
[55] J. Zhou, Y. Wang, C. Liao, B. Sun, J. He, G. Yin, S. Liu, Z. Li, G. Wang, X. Zhong, J. Zhao, *Sens. Actuators, B* **2015**, *208*, 315.
[56] L. V. Nguyen, K. Hill, S. Warren-Smith, T. Monro, *Sens. Actuators, B* **2015**, *221*, 320.
[57] F. Xia, Y. Zhao, Y. Peng, *Sens. Actuators, A* **2020**, *301*, 111754.
[58] M. Zhu, M. Z. Lerum, W. Chen, *Langmuir* **2012**, *28*, 416.
[59] A. Guglya, E. Lyubchenko, in *Emerging Applications of Nanoparticles and Architecture Nanostructures* (Eds.: A. Barhoum, A. S. H. Makhlouf), Elsevier, Amsterdam **2018**, pp. 95–119.